

A NEW EMPIRICAL METALLICITY CALIBRATION FOR VILNIUS PHOTOMETRY

S. Bartašiūtė, S. Raudeliūnas and J. Sperauskas

Astronomical Observatory of Vilnius University, Čiurlionio 29, Vilnius, LT-03100, Lithuania

Received: 2013 August 7; accepted 2013 November 29

Abstract. We present a new calibration of the seven-color Vilnius system in terms of $[\text{Fe}/\text{H}]$, applicable to F–M stars in the metallicity range $-2.8 \leq [\text{Fe}/\text{H}] \leq +0.5$. We employ a purely empirical approach, based on ~ 1000 calibrating stars with high-resolution spectroscopic abundance determinations. It is shown that the color index $P-Y$ is the best choice for a most accurate and sensitive abundance indicator for both dwarf and giant stars. Using it, $[\text{Fe}/\text{H}]$ values can be determined with an accuracy of ± 0.12 dex for stars of solar and mildly sub-solar metallicity and ± 0.17 dex for stars with $[\text{Fe}/\text{H}] < -1$. The new calibration is a significant improvement over the previous one used to date.

Key words: techniques: photometric – stars: fundamental parameters – stars: abundances – stars: metallicity calibration

1. INTRODUCTION

Metallicity estimation from broad- and intermediate-band photometry is a very practical and efficient means to obtain metal abundances for large samples of faint stars. Such methods are based on the sensitivity of stellar color indices to photospheric abundances over a relatively wide wavelength range. Techniques for deriving metallicity parameters $[\text{Fe}/\text{H}]$ were developed and are used in a number of photometric systems, e.g., *Sloan*, *wvby*, *UBV*, *DDO*, etc.

The metal abundance sensitivity of the seven-color *Vilnius* system *UPXYZVS* was first demonstrated in the papers by Bartkevičius & Straizys (1970a,b). This system (for its details, see Straizys 1992) includes several color indices in the region $\sim 3200-4800$ Å, shown to be most effective at differentiating the metallicity effect: $U-X$, $U-Y$, $P-X$, $P-Y$ and $X-Y$. Later on, Bartkevičius & Sperauskas (1983; hereafter BS83) calibrated empirically three of the above-quoted color indices in terms of $[\text{Fe}/\text{H}]$ by using 133 field stars with known values of metallicity, but only half of these stars then had $[\text{Fe}/\text{H}]$ values from high-dispersion spectroscopy. Their calibration of $P-Y$ and $X-Y$ applies to dwarf stars of spectral types F0–K4 in the metallicity range from +0.5 to –2.5 dex and that of $P-X$, $P-Y$ and $X-Y$ applies to giant stars of types F8–M4 in the $[\text{Fe}/\text{H}]$ range from +0.5 to –3.0 dex. The order of accuracy of the BS83 calibration is about ± 0.20 dex in $[\text{Fe}/\text{H}]$.

Since the publication of BS83, a fair amount of observational data have been

accumulated, both in the *Vilnius* system and from high-dispersion spectroscopy. This permits a much-improved recalibration of *Vilnius* photometry. Such a need has become increasingly important in the light of recent photometric CCD surveys in the *Vilnius* system, which have substantially increased the quality and volume of photometric data available for the Milky Way clusters and field stars (e.g., Bartašiūtė et al. 2011; Zdanavičius et al. 2011, 2012; Straizys et al. 2013).

We have therefore undertaken a reevaluation of the original BS83 calibration and provide in this paper its updated version which keeps the same empirical approach as that used in BS83 but expands a calibrating sample to include nearly 1000 F–M stars (a seven-fold increase in sample size) with more recent [Fe/H] values from high-dispersion spectra and thus to ensure a better accuracy of metallicity estimation.

The layout of the paper is as follows. In Section 2 we describe the stellar sample and the data used for metallicity calibration. Section 3 describes details of the empirical method used and presents a new calibration for dwarfs and giant stars. In this section we compare the accuracy of the updated and original versions of calibration and discuss their implications. Conclusions and recommendations are summarized in Section 4.

2. THE SAMPLE

In any attempted metallicity calibration, it is critically important to have an extensive and homogeneous sample of spectroscopically determined abundances for stars for which there are also accurate *Vilnius* photometric data.

As a source catalog for *Vilnius* photometry the latest updated version of the *General Photometric Catalogue of Stars Observed in the Vilnius System* (Kazlauskas 2010) was used, which contains compilations from the published sources for $\sim 10\,000$ stars and supersedes the previous catalog by Straizys & Kazlauskas (1993). Only stars which have both the *Hipparcos* parallaxes and the metallicity determinations from high-dispersion spectra were extracted from this catalog. Where more than one source was available for a given star, the results of photometry were averaged. If the differences between the values of color indices from different sources exceeded 0.02 mag (in the case of non-variable stars), such averaged color indices were treated as inaccurate and not used in metallicity calibration.

The spectroscopic metallicity determinations were taken from the PASTEL catalog by Soubiran et al. (2010) and its updated version¹. The catalog supersedes the two previous versions (Cayrel de Strobel et al. 1997, 2001) and provides the most recent compilation of [Fe/H] determinations obtained from detailed analysis of high resolution, high S/N spectra, together with the atmospheric parameters T_e and $\log g$, spectral types and bibliographic references. For a small number of stars, [Fe/H] determinations from high-dispersion spectra were found in the very recent literature sources not yet included in the updated PASTEL version (e.g., Afsar et al. 2012). Since the metallicity determinations in the PASTEL compilations come from a variety of sources it was not possible to claim zero point offsets between the metallicity scales. Therefore, we took from PASTEL the values of [Fe/H] without any change in zero-points. In the case of multiple [Fe/H] determinations, we adopted [Fe/H] values averaged over different sources (no weights were attached

¹ <http://vizier.u-strasbg.fr/viz-bin/VizieR?-source=B/pastel>

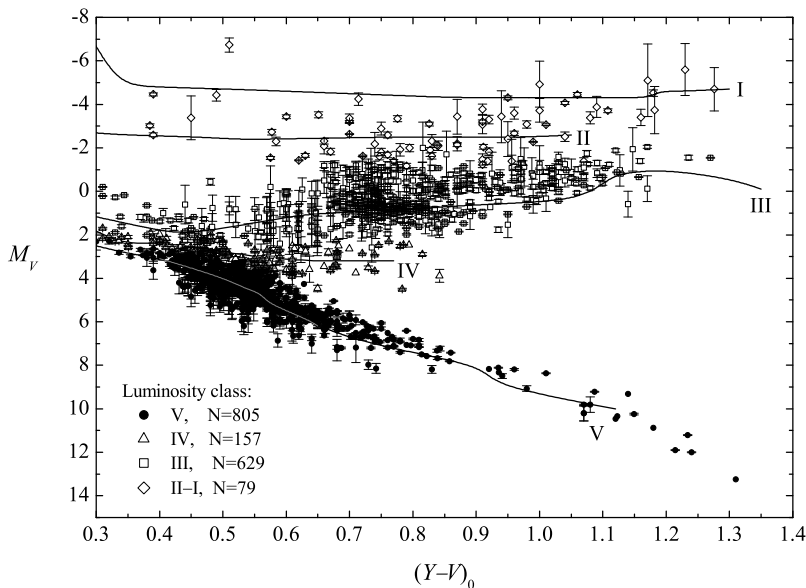


Fig. 1. M_V vs. $(Y-V)_0$ diagram for 1666 stars with metallicity estimates from high-dispersion spectra. Absolute magnitudes are calculated from Hipparcos parallaxes, with the exception of 66 stars with unacceptably large parallax errors, mainly of luminosity class III to I, for which M_V were derived from *Vilnius* photometry. The mean relations for solar composition stars of luminosity classes V to I, taken from Straižys (1992), are shown as continuous lines.

to authors of $[\text{Fe}/\text{H}]$ estimates, but only sources after 1990 were used in averaging). In the case of considerable discrepancy in the published values of $[\text{Fe}/\text{H}]$, mainly because of different effective temperatures assumed, we avoided the inclusion of such stars. We note that metallicity determinations by McWilliam (1990), given for a large number of G–K giant stars in our sample (272), were found to be systematically by 0.11 dex lower, on average, than those of the many other sources (see, also, a remark on this point by Liu et al. 2007). Since the McWilliam stars cover mostly the range $[\text{Fe}/\text{H}] > -0.5$, in which the majority of our sample stars had $[\text{Fe}/\text{H}]$ values from other sources, we did not attempt to tie the abundance scale of this particular source to some known zero-point, but excluded this source from averaging and from further calibration procedures.

The use of the Hipparcos catalog (new reduction, van Leeuwen 2007) allowed us to reliably determine distances to the calibrating stars and to check an assessment of their luminosity classes. The knowledge of accurate distances were critically important to see whether there was the need for correction of colors due to interstellar reddening or not. The stars lying at distances less than 40 pc were assumed to be free of reddening. For stars at greater distances, the values of interstellar reddening were determined using regular techniques of photometric classification in the *Vilnius* system (see, e.g., Bartkevičius & Lazauskaitė 1996 for the principle of this technique). In the case of nonzero reddening, the colors of stars were dereddened using the color excess ratios taken from Kurilienė & Sūdžius (1974) and Bartkevičius & Sviderskienė (1981) for Population I and II stars, respectively.

A total of 1666 stars were found which have both *Vilnius* photometry and

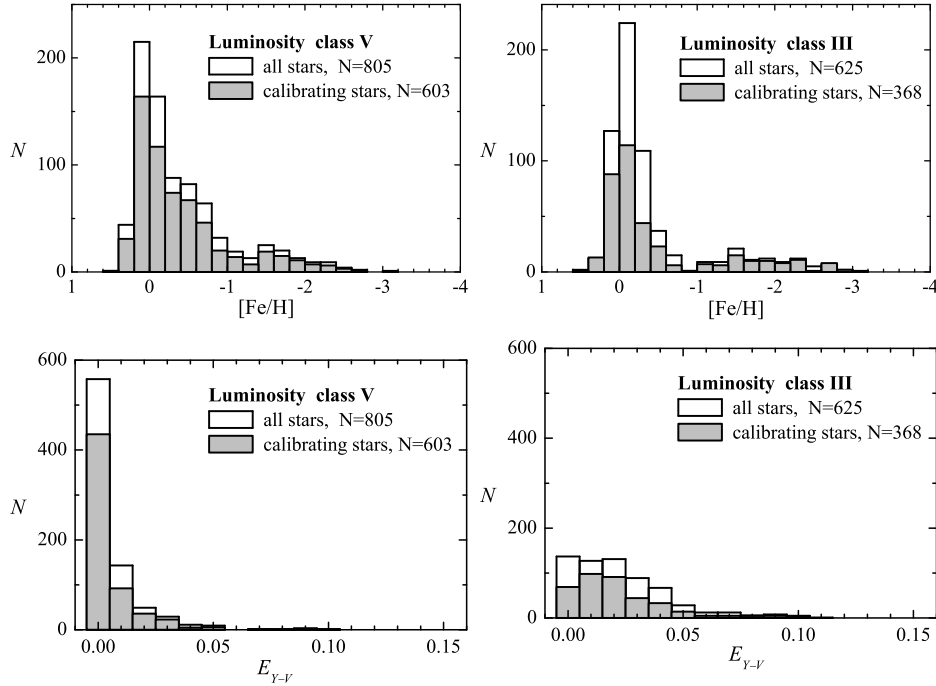


Fig. 2. Distributions of dwarf and giant stars by metallicity (top panels) and by values of interstellar reddening, E_{Y-V} (bottom panels). Unshaded histograms represent all stars in the sample, whereas shaded histograms indicate calibrating stars left after removal of binaries, variables and stars with inaccurate photometry or with discrepant values of spectroscopic $[\text{Fe}/\text{H}]$.

metallicity estimates from high-dispersion spectra. The M_V vs. $(Y-V)_0$ diagram for these stars is displayed in Figure 1. The stars of luminosity class IV (157 stars) and luminosity class II–I (79 stars) are not the subject of current metallicity calibrations and have therefore been omitted from our subsequent analysis, leaving a sample of 805 dwarf stars and 625 giant stars, which cover a range of $Y-V$ color from 0.35 to 1.3, or, spectral classes from F0 to M4. The distributions of these stars by metallicity and the values of interstellar reddening E_{Y-V} are shown in Figure 2 (unshaded histograms). As can be seen from the histograms, the range of metallicities covered is $-2.8 \leq [\text{Fe}/\text{H}] \leq +0.4$. The overwhelming majority of the dwarfs are nearby and unreddened, whereas a significant fraction of the giants are slightly reddened, having color excesses E_{Y-V} mostly less than 0.05 mag. Very few stars have slightly larger reddening values, but not exceeding 0.10 mag.

Particular attention has been paid to removing unresolved binaries from a sample of calibrating stars, which primarily affect photometric measurements, making the binary system appear brighter and redder. Consequently, certain combinations of primary and secondary stars can give quite highly erroneous photometric estimates of metallicities. We have searched for known spectroscopic binaries by making a prior cross-checking of our sample of dwarf and giant stars with the catalog of spectroscopic binaries by Pourbaix et al. (2004–2009) and with the catalogs of radial velocities by Nidever et al. (2002), Famaey et al. (2005) and Nordstrom

et al. (2004). Also, the Simbad database and the *Hipparcos* catalog entries for all of the stars were checked to avoid the inclusion of any double stars. The known binaries and radial-velocity variables comprise 20% and 17% of our subsamples of dwarf and giant stars, respectively. These were excluded from calibration procedures. However, some unrecognized double stars can almost certainly remain in our cleaned sample.

The known variable stars in the sample have been searched by cross-checking with the *General Catalog of Variable Stars* (Samus et al. 2007–2012); these constitute 17% of the sample, with nearly one third of them known also as spectroscopic binaries. Only those which were known to exhibit low-level (≤ 0.02 mag) variability were admitted to the final sample to be used in metallicity calibration.

After excluding known binaries, variable stars, carbon and Ba stars (most of which are also spectroscopic binaries) and also stars with less accurate photometry (differences in color indices between different sources ≥ 0.03 mag) or discrepant values of $[\text{Fe}/\text{H}]$, we retained in our final sample for metallicity calibration 603 dwarfs and 368 giants. Their distributions by $[\text{Fe}/\text{H}]$ and reddening values E_{Y-V} are shown by shaded histograms in Figure 2.

3. METALLICITY CALIBRATIONS

3.1. Method

In this paper, we used the same empirical approach as that given in BS83, which is based on the method put forward by Bond (1980) for metallicity calibration of the *Strömgen* m_1 index. Here, we will only briefly describe the main points of the method.

Line weakening or strengthening due to the effects of metallic lines in stellar atmospheres (line blanketing) can be measured by the color excess $\delta(CI)$ defined as the difference between a star’s metallicity-sensitive color index CI and the same color index that this star would have if its metallicity were exactly solar ($[\text{Fe}/\text{H}]=0.00$); we shall label the latter $(CI)_n$. In a two color diagram with a temperature-dependent color index plotted on the x -axis, $\delta(CI)$ is a height of a star’s point above (or below) the solar-composition relation. However, we cannot use a simple linear relation between $\delta(CI)$ and $[\text{Fe}/\text{H}]$, since the abundance sensitivity of a color index is not the same for different intervals of effective temperature. This effect is mostly attributable to a progressive increase of line blanketing with decreasing temperature. Instead, a more relevant quantity $\delta'(CI)$, introduced originally by Bond (1980), can be used, which was also employed in the calibration by BS83. In a two color diagram, $\delta'(CI)$ defines the above described excess $\delta(CI)$ in units of the distance $\delta(CI)_{\text{max}}$ between the solar composition relation and the line of some fixed maximal metal-deficiency $(CI)_{\text{max}}$ at the same temperature:

$$\delta'(CI) = \frac{\delta(CI)}{\delta(CI)_{\text{max}}}, \quad (1)$$

where $\delta(CI) = (CI)_n - (CI)$ and $\delta(CI)_{\text{max}} = (CI)_n - (CI)_{\text{max}}$. Having the values of $\delta'(CI)$ calculated for a sample of stars with accurate spectroscopic metallicities the remaining step of calibrations is to find a relation between $\delta'(CI)$ and $[\text{Fe}/\text{H}]$.

To calculate $\delta'(CI)$ properly, we need to know the two-color relations defining both the $[\text{Fe}/\text{H}]=0$ isoline and the isoline of maximal metal-deficiency. The easiest

way would be to use stellar models computed for the *Vilnius* system. However, despite improvements in theoretical models, it does not appear that the transformations from theoretical to observational colors are yet sufficiently reliable. A comparison in the two-color diagrams of the loci of sequences of real stars with those from a widely used grid of Kurucz (2001) model atmospheres², computed for the *Vilnius* system, demonstrated that model colors do not adequately match the observational data even in the case solar metallicity stars (see Figures 4 and 6 and remarks in § 3.2 and 3.3). Therefore, we derived the metallicity dependent color shifts $\delta'(CI)$ empirically, i.e. relying solely on observational data.

As in the BS83, we used three types of two-color diagrams, $(P-X, Y-V)$, $(P-Y, Y-S)$ and $(X-Y, Y-V)$, where $P-X$, $P-Y$ and $X-Y$ are metallicity indicators and $Y-V$ and $Y-S$ are effective-temperature indicators which are almost insensitive to blanketing. We made no attempt to calibrate the color indices including ultraviolet magnitude, $U-X$ and $U-Y$, because they are most sensitive to the effects of luminosity. As color indices $P-X$, $P-Y$ and $X-Y$ are also susceptible to luminosity, the relations between $\delta'(CI)$ and $[Fe/H]$ were obtained for dwarf and giant stars separately. Before computing $\delta'(CI)$, the observed color indices were corrected for interstellar reddening, if needed. Throughout this paper, the notations $(CI)_0$ or CI always denote intrinsic color indices.

As a first step, a standard empirical relation for solar composition stars in the two-color stars diagrams was defined using our sample stars within ± 0.10 dex of the solar $[Fe/H]$. However, the small number of stars earlier than F2 and later than M0 complicated the determination of the relation near both ends of the spectral range of interest. Therefore we selected from the catalog of *Vilnius* photometry an additional number of stars with determined (mainly by the BS83 technique) photometric metallicities within ± 0.15 dex (a less restricted interval chosen to allow for the effect of errors in photometric $[Fe/H]$ determinations). Since their loci in the two-color diagrams are quite compatible with those of a few solar-metallicity stars, known from high-dispersion spectroscopy (see Figures 4 and 6), we included these additional stars in defining the ends of the relation, which refer to the spectral intervals earlier than F2 ($Y-V < 0.4$) and later than $\sim M0$ ($Y-V > 0.9$ for dwarfs and $Y-V > 1.2$ for giants).

Next, in the two-color diagrams, the mean line for a maximal metal-deficiency, $(CI)_{\max}$, has to be defined, within which our calibrations should be valid (i.e., $[Fe/H]$ close to -3.0 dex). Since in general we do not have sufficient observational data on extremely metal-poor stars over the entire $Y-V$ color range we are considering, it was not possible to define this line simply as an upper envelope of the points in the two-color diagrams. To overcome this problem, we adopted here the following approach. Since, at a fixed metallicity, $\delta'(CI)$ should essentially be the same throughout the $Y-V$ color range, the formula (1) can be used to extract the shifts $\delta(CI)_{\max}$, and hence to calculate $(CI)_{\max}$, using a mean two-color relation defined for stars of the same metal-deficiency if only its corresponding quantity $\delta'(CI)$ is known at any (at least one) fixed color $Y-V$. Therefore, we chose fixed values of $Y-V$ in the regions of the two-color diagrams, where the calibrating stars cover the entire range of $[Fe/H]$, and estimated the empirical dependence of color indices on $[Fe/H]$ as illustrated in Figure 3. Then, the dependence of each color index considered was extrapolated down to an arbitrary metallicity of -3 dex to

² <http://kurucz.harvard.edu/grids.html>

yield, at a given $Y-V$, an estimate of $\delta(CI)_{\max}$ and, from formula (1), the quantities $\delta'(CI)$'s across this range of metallicity. Using the empirical lines drawn in the two-color diagram through the points of stars with closely similar metal-deficiency (e.g., -0.5 , -1.2 , -1.5 , ..., -2.0 dex), or, when the observational data were insufficient, using only segments of such lines, and having the quantities $\delta'(CI)$ we obtained by formula (1) a set of $(CI)_{\max}$ lines, which, in the ideal case, should coincide. Taking their average position in the two-color diagram, the final $(CI)_{\max}$ line was constructed over a wide range of $Y-V$ (or $Y-S$).

The two-color relations defining the $[\text{Fe}/\text{H}]=0$ isoline, $(CI)_n$, and the isoline of maximal metal-deficiency, $(CI)_{\max}$, are tabulated in Appendix. The two-color diagrams with these empirical relations are shown in Figures 4 and 6 for dwarfs and giant stars, respectively, and will be briefly discussed in the next two subsections.

3.2. Dwarf stars

All the dwarfs in our sample are specifically chosen to be unevolved stars, ensured by the requirement that their *Hipparcos*-based absolute magnitudes M_V should all be within the expected limits of the main sequence (Figure 1). We divided the sample stars into five metallicity groups and plotted the two-color diagrams in Figures 4 a,b,c. All symbols, except for small thin crosses, indicate stars having $[\text{Fe}/\text{H}]$ estimates from high-dispersion spectra. The heavy continuous line is the mean relation for solar-metallicity stars, drawn through the points representing stars in the range $+0.10 \geq [\text{Fe}/\text{H}] \geq -0.10$ (solid dots); due to insufficient number of stars of certain spectral types, a number of additional stars which had only photometric metallicity estimates or, in the case when $Y-V > 0.75$, otherwise classified as normal chemical composition stars, were also included in the fit (these stars are shown as small thin crosses). Thin continuous line is the $(CI)_{\max}$ line defined in this paper (see § 3.1 for details). Shown in Figures 4 b,c as thin dashed line is the $(CI)_{\max}$ relation used in the previous calibration by BS83. Theoretical curves of Kurucz (2001) models (dashed-dot lines) are shown for $[\text{Fe}/\text{H}] = -3.0$ (upper line), 0.0 dex (middle line) and $+1.0$ dex (bottom line). We did not remove from the plots known binaries and variable stars, therefore part of the scatter within each group may be due to differences other than metallicity.

The rms scatter about each of the three two-color relations defined for solar-metallicity stars of spectral types earlier than K4 ($Y-V \leq 0.75$) varies from ± 0.02

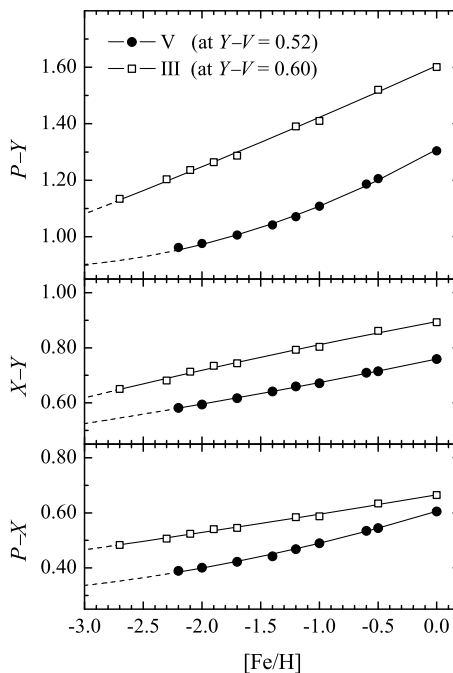


Fig. 3. Dependence of the metallicity-sensitive color indices on $[\text{Fe}/\text{H}]$ at a fixed value of $Y-V$ for luminosity classes V and III.

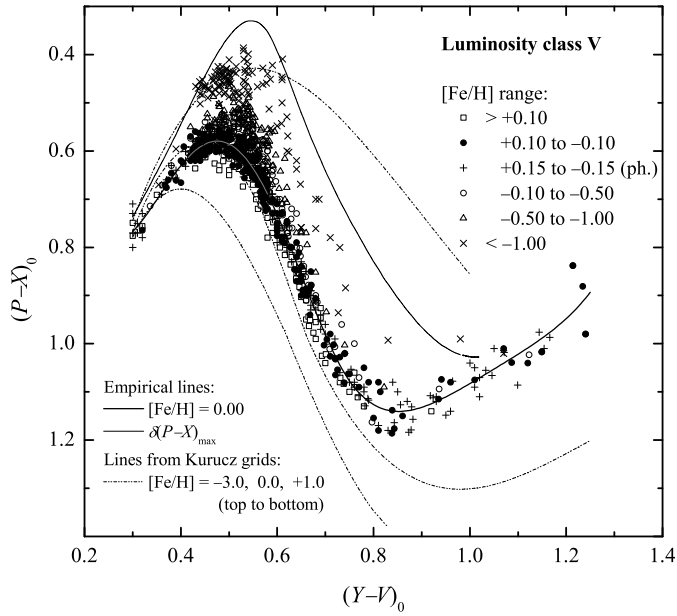


Fig. 4a. $(P-X, Y-V)$ diagram for dwarf stars. Symbols indicate stars having $[\text{Fe}/\text{H}]$ estimates from high-dispersion spectra, except for small thin crosses, which indicate stars having only photometric $[\text{Fe}/\text{H}]$. For more explanations, see text in § 3.2.

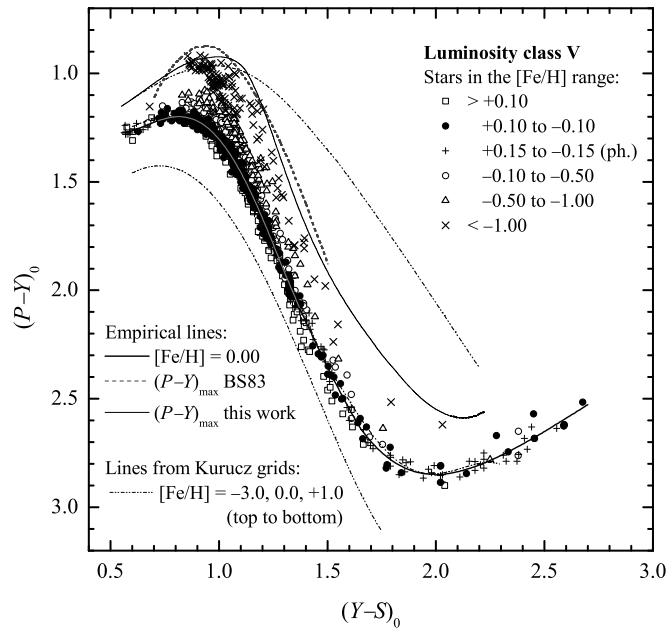


Fig. 4b. $(P-Y, Y-S)$ diagram for dwarf stars. Symbols and lines the same as in Fig. 4a. Shown as dashed line is the $(P-Y)_{\text{max}}$ relation defined by BS83.

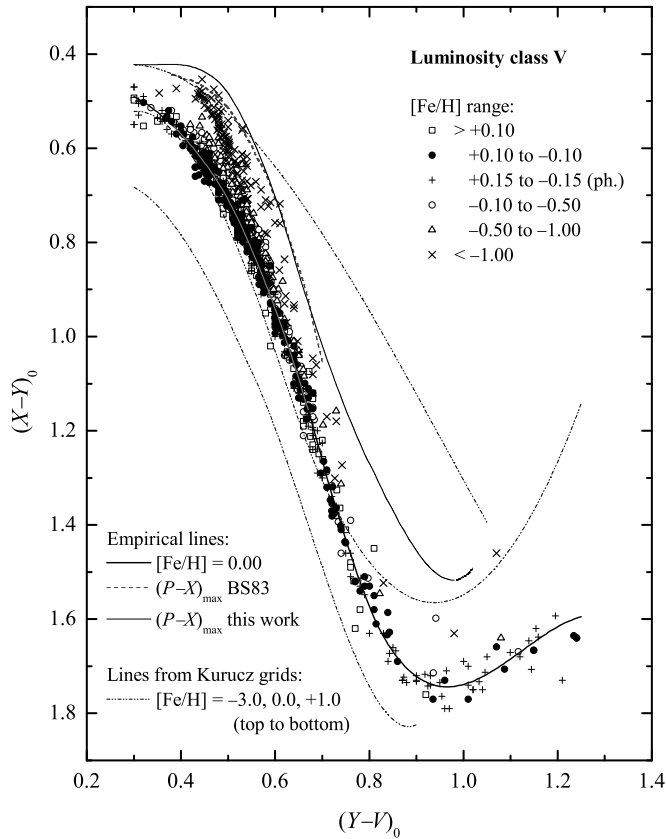


Fig. 4c. $(X-Y, Y-V)$ diagram for dwarf stars. Symbols and lines the same as in Figs. 4 a,b.

for $P-X$ and $X-Y$ to ± 0.03 for $P-Y$. For $Y-V > 0.75$ (spectral types K5–M4), the scatter is larger, ± 0.03 for $P-X$ and ± 0.04 for $X-Y$ and $P-Y$. We note that over most of the temperature range considered the defined solar-metallicity relations match quite well the mean relations given by Straižys (1992; Table 66) for dwarfs of normal chemical composition (the latter relations are not displayed in Figures 4 a,b,c in order to prevent an overlap of the lines). A comparison of the empirical $[\text{Fe}/\text{H}] = 0$ relations with the theoretical curves from Kurucz (2001) models computed for the *Vilnius* system indicates a satisfactory match only in the case of $(P-Y, Y-S)$ diagram. In the $(P-X, Y-V)$ and $(X-Y, Y-V)$ diagrams, model colors are clearly shifted relative to the observational sequences, with the most obvious cases of disagreement occurring in the region of late K and M dwarfs.

From the spread of points denoting subdwarfs it is clearly seen that the maximal deblanketing for the color index $P-Y$ is about twice as large as that for indices $P-X$ and $X-Y$ (notice that in the figures the axes scales also differ twice, but in the opposite sense). The $(CI)_{\text{max}}$ lines defined in this paper (thin continuous line in Figures 4 a, b, c) are generally close to those adopted in BS83 (thin dashed line in Figures 4 b,c; for $P-X$, BS83 gave no calibration), but extend significantly the

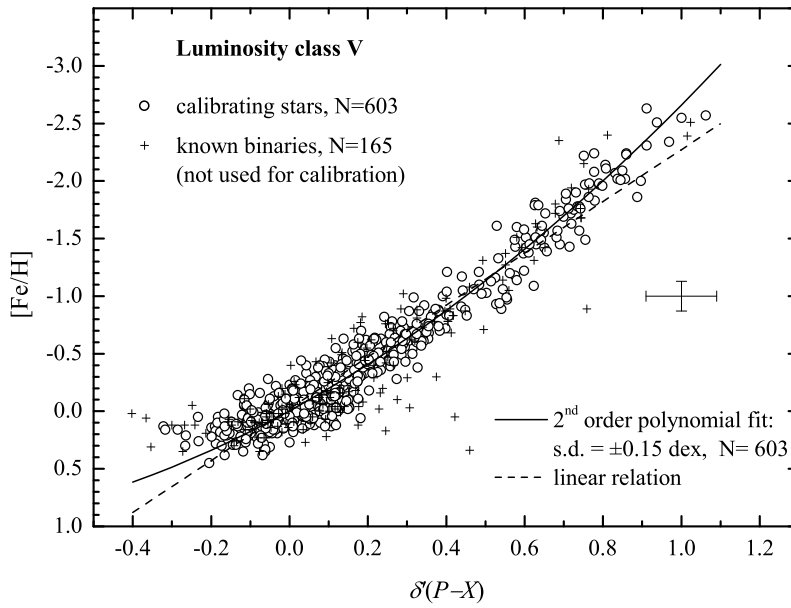


Fig. 5a. $\delta'(P-X)$ vs. $[Fe/H]$ relation for calibrating dwarf stars with metallicities from high-dispersion spectroscopy. The solid line is a second-order polynomial fit and the dashed line is a linear relation. Known spectroscopic binaries are plotted for comparison.

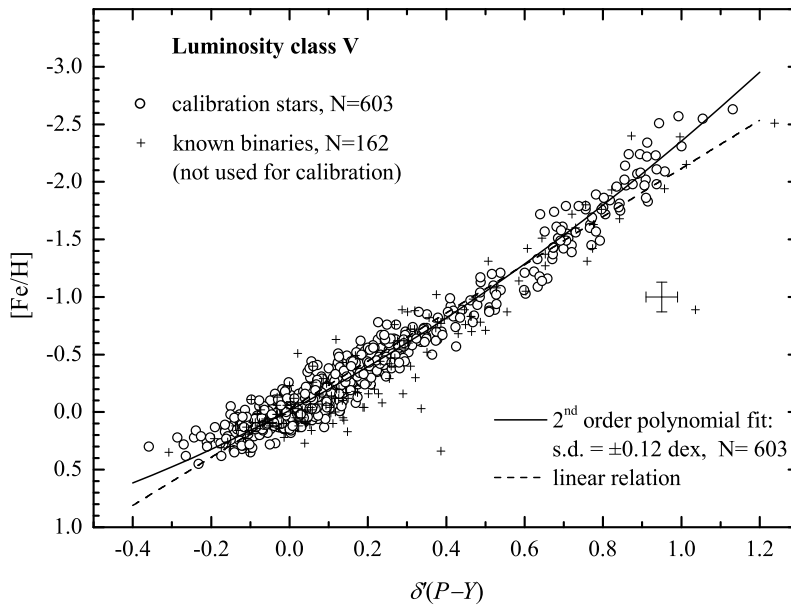


Fig. 5b. $\delta'(P-Y)$ vs. $[Fe/H]$ relation for calibrating dwarf stars with metallicities from high-dispersion spectroscopy.

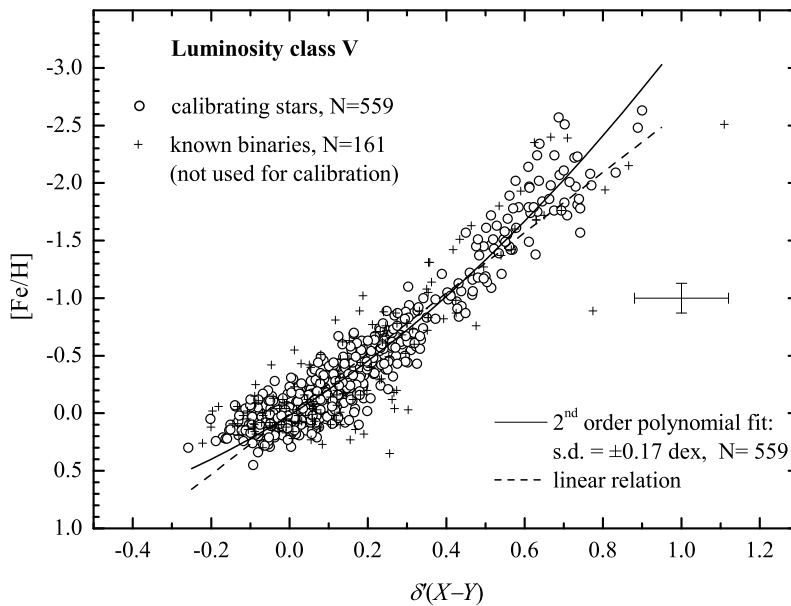


Fig. 5c. $\delta'(X-Y)$ vs. $[Fe/H]$ relation for calibrating dwarf stars with metallicities from high-dispersion spectroscopy.

spectral range covered to later types. However, due to the very few subdwarfs of late K and M types in the sample, the extension of our empirical $(CI)_{\max}$ line to the M-type region should be considered as very provisional. Despite the fact that the $(CI)_{\max}$ line was constructed in such a way that it should approximately represent a -3.0 dex metallicity, its position in either of the three diagrams differs significantly from the -3.0 dex model curve. It should be noted in this context that the existence of large differences between observed and synthetic *Vilnius* colors for Kurucz models was earlier shown by Straižys et al. (2002). At the early-spectral-type end (A8–F0) of the two-color diagrams, where the lack of subdwarfs in the sample prevented extension of the $(CI)_{\max}$ line into this region, this line was extrapolated to the bluest point of the -3.0 dex model curve.

In Figures 5a,b,c we plot for the calibrating dwarfs the quantities $\delta'(P-X)$, $\delta'(P-Y)$ and $\delta'(X-Y)$ versus $[Fe/H]$ from high-dispersion spectroscopy. The error bars shown in each diagram are estimates of the average standard deviation in the spread in $[Fe/H]$ from multiple determinations (± 0.13 dex) and the error of $\delta'(CI)$, produced by uncertainties in photometry, interstellar-reddening corrections and two-color relations. As it was mentioned in § 2, known binaries and variable stars were excluded from the calibrations. In Figures 5a,b,c we plotted these stars (marked by thin crosses) just to illustrate the scatter contributed by the effects of binarity. A few binary stars deviating very significantly on the lower right of the relation are also known as variables of RS CVn and other types. In general, a large fraction of spectroscopic binaries still fall in the region of calibrating stars.

To obtain the equations of $\delta'(CI)$, $[Fe/H]$ relations, a second-order polynomial was fitted via a least-squares fitting routine, although a major part of the relation, as can be seen in Figures 5a,b,c, is actually almost linear. Only near both ends of

the metallicity range, $[\text{Fe}/\text{H}] < -1.5$ and $[\text{Fe}/\text{H}] > 0$, a departure from linearity is obvious, which may indicate a decreased metallicity sensitivity of the color indices. For the metal-rich end of the relation there might also be some other reasons. Polynomial coefficients of the relations and their errors are given in Table 1.

A comparison of Figures 5 a,b,c (see also Table 1) indicates that the calibration of color indices $P-X$ and $P-Y$ is more accurate than that of $X-Y$. The rms deviations of the standard $[\text{Fe}/\text{H}]$ values from the fits are ± 0.17 dex for $X-Y$, ± 0.15 dex for $P-X$ and only ± 0.12 dex for $P-Y$. This result confirms the conclusion drawn from the earlier investigation by Bartkevičius & Straizys (1970 a) that the color index $P-Y$ shows the largest deblanketing effect and is most suitable for estimating metallicity of subdwarf stars.

As a final estimate of photometric metallicity of dwarfs and subdwarfs, we recommend to use primarily the result based on $P-Y$ or to use an average over the results from $P-Y$ and $P-X$, weighted in favor of $P-Y$. The color index $X-Y$ can be used as an additional means of lower weight. The calibration is applicable to dwarf stars of spectral types $\sim \text{A8}$ to M1 ($Y-V = 0.30-1.02$, or $Y-S = 0.55-2.22$) and the metallicity range $-2.8 < [\text{Fe}/\text{H}] < +0.5$. The accuracy of the calibration and a comparison with BS83 will be discussed in § 3.4.

3.3. Giant stars

The same procedure, as described in the previous subsection, we repeated for giant stars. The three two-color diagrams, on which our calibrations were based, are displayed in Figures 6 a,b,c. The diagrams contain the same information as Figures 4 a,b,c.

As in the case of dwarf stars, the empirical $[\text{Fe}/\text{H}]=0$ relations were determined using stars with $+0.10 \geq [\text{Fe}/\text{H}] \geq -0.10$ from high-dispersion spectra, plus an additional number stars without spectroscopic metallicities (in the figures marked by small thin crosses) to smooth out the very sparse sampling near the ends of the spectral-type range. The standard deviation around these relations is ± 0.02 mag. A comparison with the canonical relations for normal chemical composition stars of luminosity class III, given by Straizys (1992; Table 68), revealed no significant differences.

Model curves from Kurucz's grids for $[\text{Fe}/\text{H}]=0$, again, do not satisfactorily match the empirical relations, except for the $(P-Y, Y-S)$ diagram where both curves, theoretical and empirical, show a remarkable coincidence for $Y-S < 1.4$. The model $[\text{Fe}/\text{H}]=-3.0$ line (dash-dot-dot) follows quite closely the empirical $(CI)_{\text{max}}$ line (i.e., “-3 dex isoline”) in the $(P-X, Y-V)$ diagram, as well as does over the range of spectral types earlier than K3 in the other two diagrams. Our $(CI)_{\text{max}}$ lines are very close to those defined in BS83, but are extended to include earlier spectral types. As in the case of dwarf stars, the $(CI)_{\text{max}}$ line at the early-spectral-type end was forced to fit the -3.0 dex model curve.

The calibrations of $\delta'(CI)$ are presented in Figures 7 a,b,c. The first feature to notice in these figures is the absence of calibrating stars in the region around $[\text{Fe}/\text{H}] = -1$ dex. It seems likely that this gap, also obvious in histograms of Figure 2, or, in the two-color plots in Figure 6, reflects a paucity of stars around the metallicity separating disk and halo populations rather than a sample bias (this observational fact has long been noted in the literature, see, e.g. Marsakov & Suchkov 1977). As in similar plots for the dwarf stars, known and suspected binaries (spectroscopic, astrometric, radial-velocity variables) are also plotted for

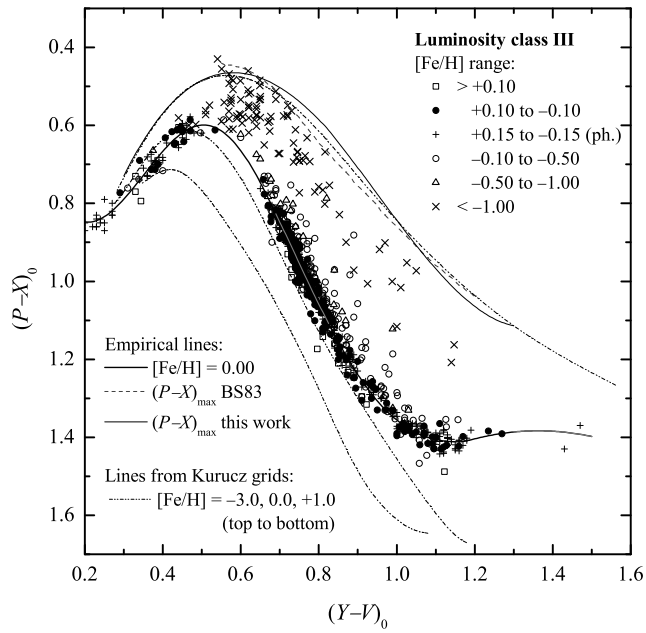


Fig. 6a. $(P-X, Y-V)$ diagram for giant stars. Symbols the same as in Figs. 4 a,b.

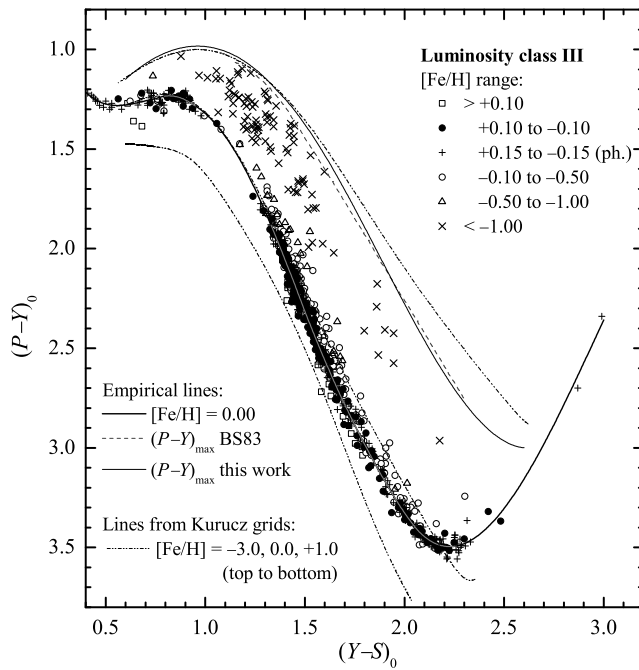


Fig. 6b. $(P-Y, Y-S)$ diagram for giant stars. Symbols the same as in Figs. 4 a,b.

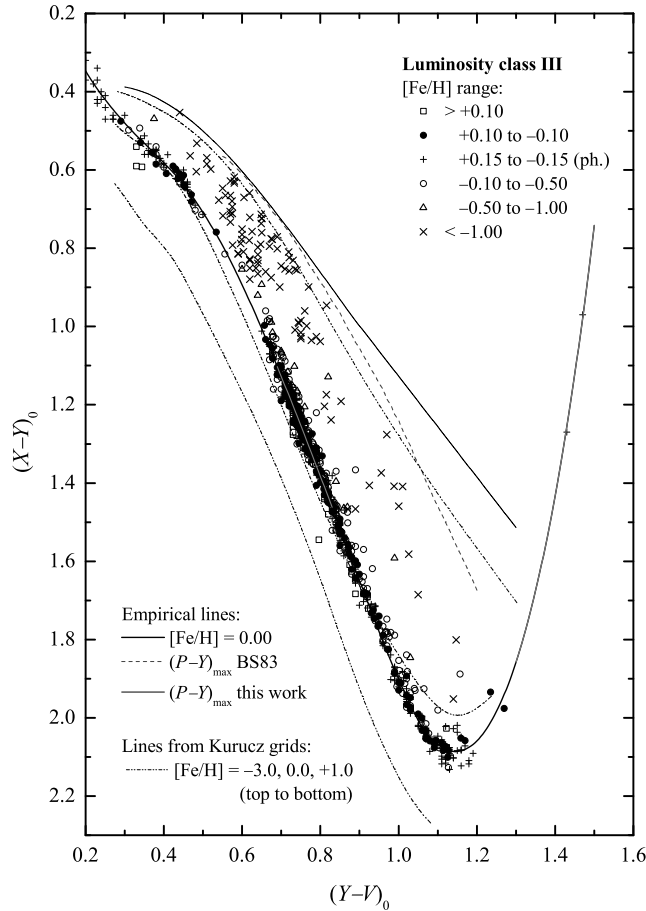


Fig. 6c. $(X-Y, Y-V)$ diagram for giant stars. Symbols as in Figs. 4 a,b.

comparison. In this context, it is interesting to note that the points denoting binary stars exhibit much less scatter in the case of $\delta'(P-Y)$ (Figure 7 b) compared to that for $\delta'(P-X)$ and $\delta'(X-Y)$ (Figures 7 a,c).

In all three plots we have almost a linear dependence of $\delta'(CI)$ on $[Fe/H]$, especially in the case of $\delta'(X-Y)$, $[Fe/H]$ relation. However, a 2nd-order polynomial fit gives a somewhat better fit to the data (the polynomial coefficients and their errors are given in Table 1). At low metallicities, the straight line in Figures 7 a,b,c declines up very slightly, what indicates that reduction in metal content down to nearly -3 dex does not significantly affect the colors of giant stars, or, at least, affects the colors less than those of metal-poor subdwarfs.

The scatter around the defined relations $\delta'(CI)$, $[Fe/H]$ is ± 0.17 dex for $P-X$, ± 0.15 dex for $X-Y$ and only ± 0.13 dex for $P-Y$. As in the case of dwarf stars, the color index $P-Y$ can be most accurately calibrated in terms of $[Fe/H]$. A somewhat less accurate relation was obtained for $P-X$ and $X-Y$, but the rms deviations are in general closely the same as in the calibration for dwarf stars. The new calibration

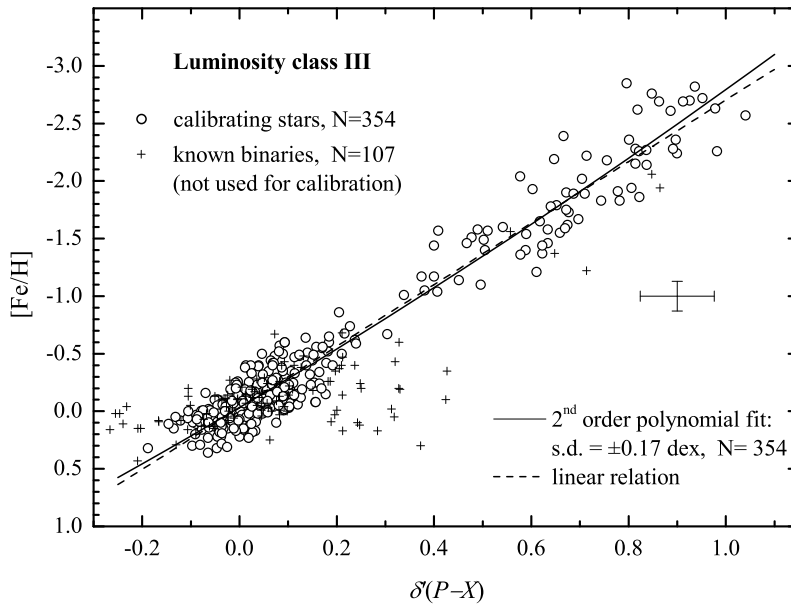


Fig. 7a. $\delta'(P-X)$ vs. $[Fe/H]$ relation for calibrating giant stars with metallicities from high-dispersion spectroscopy. The solid line is a second-order polynomial fit and the dashed line is a linear relation. Known spectroscopic binaries are plotted for comparison.

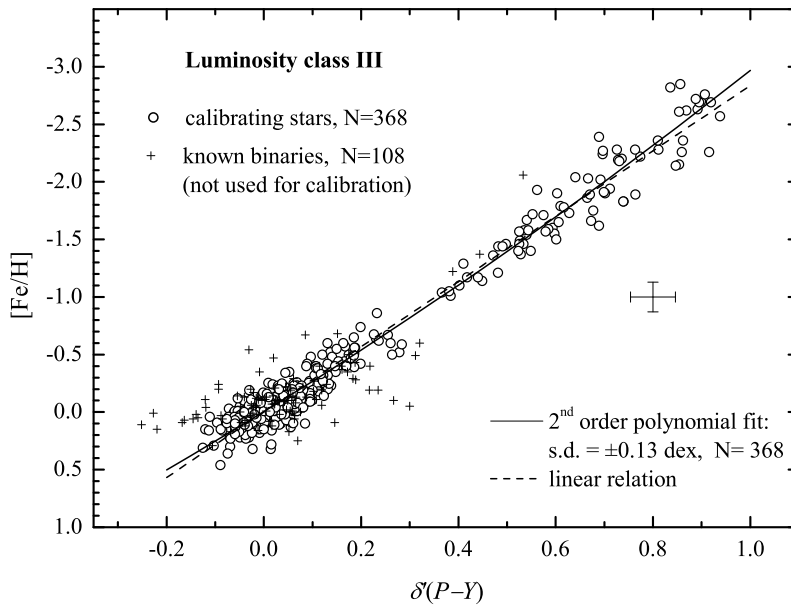


Fig. 7b. $\delta'(P-Y)$ vs. $[Fe/H]$ relation for giant stars with metallicities from high-dispersion spectroscopy.

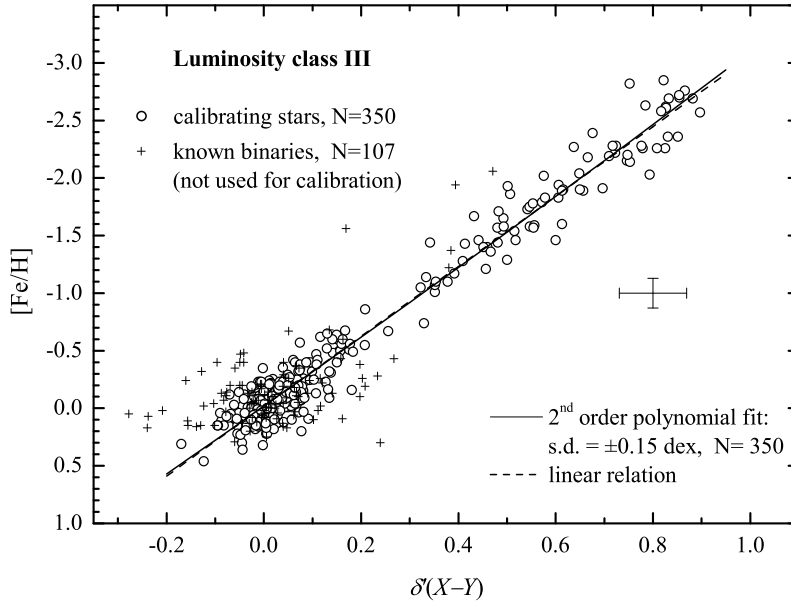


Fig. 7c. $\delta'(X-Y)$ vs. $[\text{Fe}/\text{H}]$ relation for giant stars with metallicities from high-dispersion spectroscopy.

for giants is valid in the spectral-type range $\sim A8$ to $M4$ ($Y-V = 0.30-1.30$, or $Y-S = 0.60-2.60$) and the metallicity range $-2.8 < [\text{Fe}/\text{H}] < +0.5$. The accuracy of the calibration and a comparison with BS83 will be discussed in the next subsection.

Table 1. Polynomial coefficients of the empirical relations $[\text{Fe}/\text{H}] = a_0 + a_1\delta'(CI) + a_2(\delta'(CI))^2$ for stars of luminosity class V and III. N is the number of stars used in the fits, the errors in the last column are standard deviations from the polynomial fits.

Luminosity class	$\delta'(CI)$	a_0	a_1	a_2	N	s.d. (dex)
V	$\delta'(P-X)$	-0.003 ± 0.007	-1.865 ± 0.048	-0.792 ± 0.069	603	± 0.15
V	$\delta'(P-Y)$	-0.014 ± 0.006	-1.794 ± 0.038	-0.546 ± 0.050	603	± 0.12
V	$\delta'(X-Y)$	0.018 ± 0.009	-2.132 ± 0.074	-1.131 ± 0.122	559	± 0.17
III	$\delta'(P-X)$	-0.032 ± 0.011	-2.497 ± 0.110	-0.264 ± 0.139	354	± 0.17
III	$\delta'(P-Y)$	-0.004 ± 0.008	-2.603 ± 0.083	-0.360 ± 0.110	368	± 0.13
III	$\delta'(X-Y)$	-0.019 ± 0.009	-2.968 ± 0.105	-0.113 ± 0.144	350	± 0.15

3.4. Comparison to BS83 and error analysis

In Figures 8 and 9 we compare the differences between $[\text{Fe}/\text{H}]$ from high-dispersion spectroscopy and $[\text{Fe}/\text{H}]$ determined from old (BS83) and new calibrations for the stars in our sample, plotted as functions of metallicity (left-hand panels) and the temperature-dependent color indices $Y-V$ or $Y-S$ (right-hand panels). The residuals $\Delta[\text{Fe}/\text{H}]$ plotted are in the sense “spectroscopic minus photometric”.

Consider first Figure 8, in which metallicities for stars of luminosity class V are plotted (in BS83, however, $P-X$ calibration for dwarfs was not performed). The different numbers of stars, indicated in the upper (BS83) and lower (our calibration) panels, reflect the fact that BS83 calibration covers a smaller spectral range. The figure shows that, in addition to a larger spread of residuals ($\Delta[\text{Fe}/\text{H}] \sim \pm 0.20$ dex), the old calibration of $P-Y$ and $X-Y$ systematically overestimates (by ~ 0.1 dex, on average) the metallicities over most of the $[\text{Fe}/\text{H}]$ range. There is also a systematic trend with metallicity in the results from BS83 in the range $+0.5 > [\text{Fe}/\text{H}] > -1.0$. By application of the new calibration this systematic trend disappears. Figure 8 is enough to convince one that our revised calibration for dwarfs and subdwarfs has a distinct advantage over that of BS83.

It should be noted, however, that the spread of the residuals between the values from high-dispersion spectroscopy and our photometric values is not the same over the entire range of metallicities. For stars with $[\text{Fe}/\text{H}] > -1$, the standard deviation is the same or somewhat smaller than that estimated from the whole sample of calibrating dwarfs and given in Figure 8 or Table 1. Considering only subdwarfs with $[\text{Fe}/\text{H}] < -1$ (87 stars), we estimate rms errors of ± 0.15 and ± 0.17 dex when using calibrations of $P-Y$ and $P-X$, respectively, while in the case of $X-Y$ the rms error becomes as large ± 0.24 dex (using BS83 calibration, ± 0.26 dex).

As an independent check on accuracy of our calibration for dwarf stars of chemical composition close to solar, including an estimate of the photometric metallicity zero-point error, we applied the new calibration for the Hyades dwarfs, for which *Vilnius* photometry was available. Considering a set 54 stars (excluding known spectroscopic binaries), we find an average of $[\text{Fe}/\text{H}] = +0.10 \pm 0.01$ with a dispersion of ± 0.11 dex from the $P-Y$ colors and $[\text{Fe}/\text{H}] = +0.13 \pm 0.02$ (s.d. = ± 0.15) from $P-X$. The less accurate calibration of $X-Y$ gives for the Hyades an average of $+0.10 \pm 0.03$ (s.d. = ± 0.21) dex. The average photometric metallicity values are consistent with spectroscopic estimates in the literature (e.g., Paulson et al. (2003) from a differential abundance analysis of Hyades F-K dwarfs give $[\text{Fe}/\text{H}] = +0.13 \pm 0.01$, s.d. = ± 0.05). We can therefore conclude that our new calibration seems to reproduce $[\text{Fe}/\text{H}]$ values for dwarfs of near-solar metallicity without a zero-point offset.

Let us now consider Figure 9, where comparisons are made for stars of luminosity class III. The most important feature to notice in this figure is the slope in the region $+0.5 > [\text{Fe}/\text{H}] > -1.0$, most pronounced in the distribution of points from $P-X$ and $X-Y$ calibrations. It shows that both photometric calibrations, old and new, systematically underestimate metallicities for giant stars with $[\text{Fe}/\text{H}] > 0.0$ and overestimates in the range $-0.2 > [\text{Fe}/\text{H}] > -1.0$. It is not easy to find an explanation for this discrepancy between spectroscopic and photometric $[\text{Fe}/\text{H}]$. We can suggest that at least one of the sources lies in the dependence of the color indices $P-X$ and $X-Y$ on C and N abundances. The *Vilnius* passbands P , X and Y include, in the case of late-type giants of chemical composition close to solar,

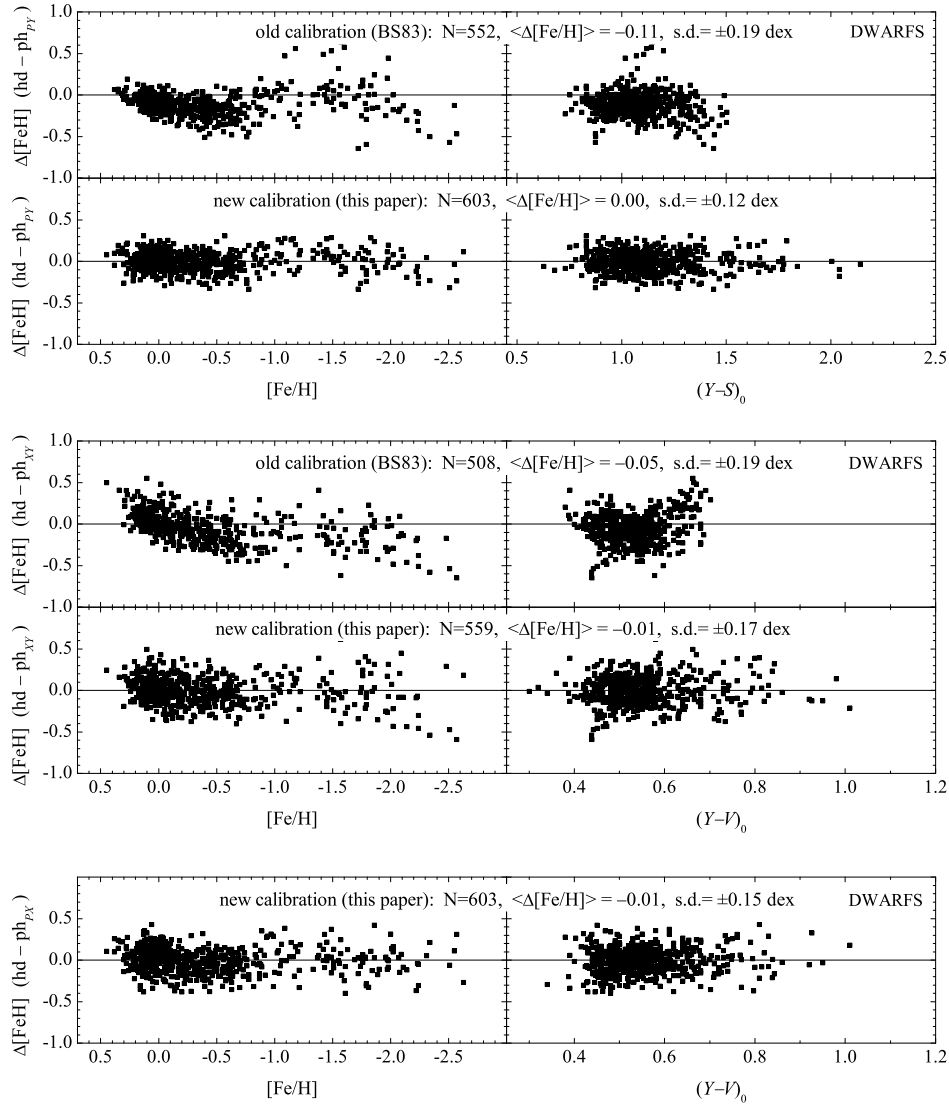


Fig. 8. Differences between $[\text{Fe}/\text{H}]$ from high-dispersion spectroscopy and $[\text{Fe}/\text{H}]$ from old (BS83) and new calibrations of *Vilnius* photometry for the same set of dwarf stars, shown as functions of $[\text{Fe}/\text{H}]$ (left-hand panels) and temperature-dependent color indices (right-hand panels). The number of stars compared, mean residuals and standard deviations are given on the top of each graph.

rather many C_2 , CH and CN molecular bands. Therefore, the corresponding color indices can predominantly be affected by the combined effect of abundances of Fe and C (and its compounds) rather than by the pure Fe abundance against which they were calibrated.

A comparison with BS83 shows that the new calibration of the color index $P-X$ shows no appreciable improvement however. In the case of $P-Y$ and $X-Y$, our

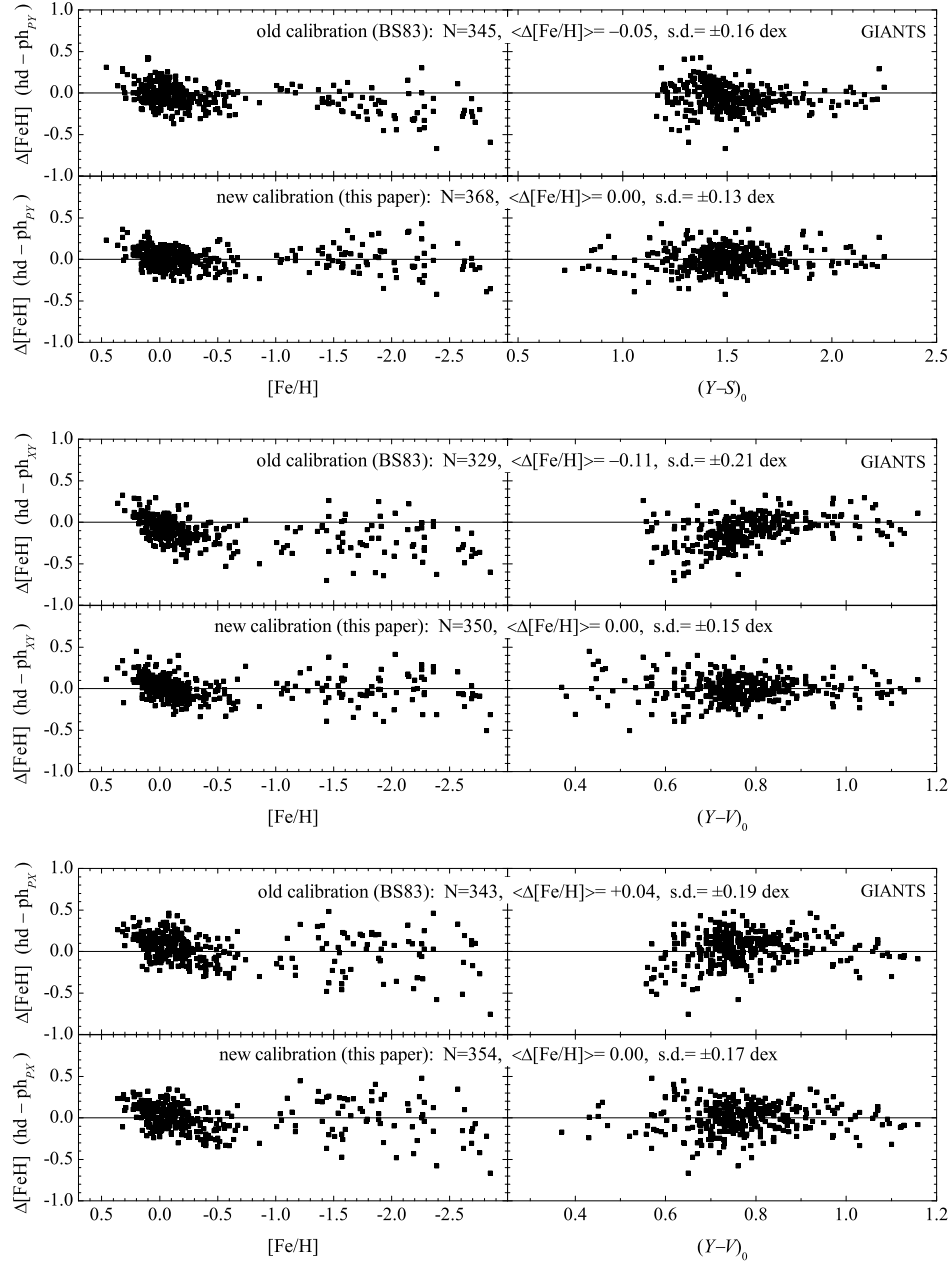


Fig. 9. Differences between $[Fe/H]$ from high-dispersion spectroscopy and $[Fe/H]$ from old (BS83) and new calibrations of *Vilnius* photometry for the same set of giant stars, shown as functions of $[Fe/H]$ (left-hand panels) and temperature-dependent color indices (right-hand panels). The number of stars compared, mean residuals and standard deviations are given on the top of each graph.

calibration has removed the systematic differences which are apparent in the ‘BS83’ metallicity values for metal-deficient giants with $[\text{Fe}/\text{H}] < -1$. For the latter stars, the new calibration of P - Y and X - Y reproduces $[\text{Fe}/\text{H}]$ values to within ± 0.17 and ± 0.18 dex, respectively, while for giants with $[\text{Fe}/\text{H}] > -1$ the rms differences from spectroscopic values become as small as ± 0.12 and ± 0.13 dex, respectively. In this metallicity range, P - X gives also satisfactory results, ± 0.15 dex, but for $[\text{Fe}/\text{H}] < -1$, our calibration of P - X can reproduce $[\text{Fe}/\text{H}]$ values only to within ± 0.25 dex (using old calibration, to ± 0.27 dex).

4. CONCLUDING REMARKS

For deriving metallicities from *Vilnius* photometry the revised empirical calibration presented here should be used, rather than the previous empirical calibration by BS83. The new calibration, based on the color indices P - X , P - Y and X - Y , is applicable to dwarf and giant stars of spectral types F-M in the metallicity range $-2.8 < [\text{Fe}/\text{H}] < +0.5$. Both for dwarfs and giants, the color index P - Y should be regarded as the most accurate and sensitive metallicity indicator. Using P - Y , $[\text{Fe}/\text{H}]$ values can be determined with an accuracy of ± 0.12 dex for stars of solar and mildly sub-solar metallicity and ± 0.17 dex for stars with $[\text{Fe}/\text{H}] < -1$. In the latter metallicity range, a more reliable estimate of photometric metallicities would be an average over the results from P - X and P - Y for dwarf stars and from P - Y and X - Y for giant stars, weighted, in either case, in favor of P - Y . For $[\text{Fe}/\text{H}] > -1$, all of the three color indices can be used, giving them proper weights.

We made no attempt to calibrate *Vilnius* color indices for stars of luminosity class IV. Subgiants in our initial sample were not numerous (a total of 157 stars), and among them only eight stars have $[\text{Fe}/\text{H}] < -1$. Instead, we would recommend for deriving their metallicities the so-called ‘comparison’ method, described in detail and applied by Bartkevičius & Lazauskaitė (1996, 1997). The principle of the method is to find from an extended data bank a set of standard stars having closely the same intrinsic color indices (or the same reddening-free parameters Q) as a star of interest and, then, to ascribe to the latter the values of $[\text{Fe}/\text{H}]$ (and other physical parameters), averaged over the extracted set standard stars. To check the validity of this approach, we compiled a data bank of 1666 stars from our sample, all with standard spectroscopic values of $[\text{Fe}/\text{H}]$, and determined by the ‘comparison’ method their metallicities. The differences from the standard $[\text{Fe}/\text{H}]$ values were found to be ± 0.16 dex for dwarfs, ± 0.19 dex for subgiants and ± 0.25 dex for subdwarfs and all giants. Although of lower accuracy than the new calibration, the ‘comparison’ method has two advantages. One is that it does not necessarily require dereddening of color indices, once the reddening-free parameters Q can be used instead of intrinsic colors. Another advantage is that it allows us to derive photometric metallicity of binary stars if a data bank of standards contains a sufficient variety of binaries. For 272 binary stars in our sample, for example, the metallicities derived by the ‘comparison’ method have a rms difference from spectroscopic values of only ± 0.20 dex.

A list of 971 calibrating stars with their parameters, used in the present work, can be supplied by authors on request.

ACKNOWLEDGMENTS. This research was supported by the Research Council of Lithuania under grant No. MIP-132/2010. The data search was greatly aided through the use of the SIMBAD database, operated at the CDS, Strasbourg.

REFERENCES

- Afsar M., Sneden C., For B.-Q. 2012, *AJ*, 144, 20
- Bartašiūtė S., Janusz R., Boyle R. P., Philip A. G. D. 2011, *Baltic Astronomy*, 20, 27
- Bartkevičius A., Lazauskaitė R. 1996, *Baltic Astronomy*, 5, 1
- Bartkevičius A., Lazauskaitė R. 1997, *Baltic Astronomy*, 6, 499
- Bartkevičius A., Sperauskas J. 1983, *Bull. Vilnius Obs.*, 63, 3 (BS83)
- Bartkevičius A., Straižys V. 1970a, *Bull. Vilnius Obs.*, 28, 33
- Bartkevičius A., Straižys V. 1970b, *Bull. Vilnius Obs.*, 30, 16
- Bartkevičius A., Sviderskienė Z. 1981, *Bull. Vilnius Obs.*, 58, 54
- Bond H. E. 1980, *ApJ*, 44, 517
- Cayrel de Strobel G., Soubiran C., Friel E. D., Ralite N., François P. 1997, *A&AS*, 124, 299
- Cayrel de Strobel G., Soubiran C., Ralite N. 2001, *A&A*, 373, 159
- Famaey B., Jorissen A., Luri X., Mayor M., Udry S., Dejonghe H., Turon C. 2005, *A&A*, 430, 165
- Kazlauskas A. 2010, *General Photometric Catalogue of Stars Observed in the Vilnius System* (in preparation), private communication
- Kurilienė G., Sūdžius J. 1974, *Bull. Vilnius Obs.*, 40, 10
- Kurucz R. L. 2001. Grids of model atmospheres (available on line at <http://kurucz.harvard.edu/grids.html>)
- Leeuwen F., van 2007, *A&A*, 474, 653
- Liu Y. J., Zhao G., Shi J. R., Pietrzyński G., Gieren W. 2007, *MNRAS* 382, 553
- Marsakov V. A., Suchkov A. A. 1977, *AZh*, 54, 1232
- McWilliam A. 1990, *ApJS*, 74, 1075
- Nidever D. L., Marcy G. W., Butler R. P., Fischer D. A., Vogt S. S. 2002, *ApJS*, 141, 503
- Nordstroem B., Mayor M., Andersen J., Holmberg J., et al. 2004, *A&A*, 418, 989
- Paulson D. B., Sneden C., Cochran W. D. 2003, *AJ*, 125, 3185
- Pourbaix D., Tokovinin A. A., Batten A. H., et al. 2004–2009, SB9: 9th Catalogue of Spectroscopic Binary Orbits
- Samus N. N., Durlevich O. V., Kazarovets E. V., Kireeva N. N., Pastukhova E. N., Zharova A. V., et al. 2007–2012, *General Catalogue of Variable Stars* (VizieR On-line Data Catalog: B/gcvs)
- Soubiran C., Le Campion J.-F., Cayrel de Strobel G., Caillo A. 2010, *A&A*, 515, A111
- Straižys V. 1992, *Multicolor Stellar Photometry*, Pachart Publishing House, Tucson, Arizona; available in pdf format from <http://www.itpa.lt/MulticolorStellarPhotometry/>
- Straižys V., Kazlauskas A. 1993, *General Photometric Catalogue of Stars Observed in the Vilnius System*, *Baltic Astronomy*, 2, 1
- Straižys V., Lazauskaitė R., Valiauga G. 2002, *Baltic Astronomy*, 11, 341
- Straižys V., Boyle R. P., Janusz R., Laugalys V., Kazlauskas A. 2013, *A&A*, 554, 3
- Zdanavičius J., Vrba F. J., Zdanavičius K., Straižys V., Boyle R. P. 2011, *Baltic Astronomy*, 20, 1
- Zdanavičius K., Straižys V., Zdanavičius J., Chmieliauskaitė R., Kazlauskas A. 2012, *A&A*, 544, 49

Appendix. The two-color relations defining the $[\text{Fe}/\text{H}]=0$ isoline, $(CI)_n$, and the isoline of maximal metal-deficiency, $(CI)_m$.

Table A1. $(P-Y, Y-S)$ relations for luminosity class V.

$Y-S$	$(P-Y)_n$	$(P-Y)_m$	$Y-S$	$(P-Y)_n$	$(P-Y)_m$
0.55	1.274	1.152	1.61	2.564	2.100
0.57	1.271	1.139	1.63	2.599	2.130
0.59	1.267	1.125	1.65	2.633	2.159
0.61	1.261	1.111	1.67	2.660	2.187
0.63	1.254	1.097	1.69	2.685	2.214
0.65	1.246	1.083	1.71	2.708	2.241
0.67	1.238	1.068	1.73	2.729	2.269
0.69	1.230	1.054	1.75	2.747	2.295
0.71	1.222	1.040	1.77	2.765	2.320
0.73	1.215	1.026	1.79	2.780	2.344
0.75	1.209	1.013	1.81	2.793	2.367
0.77	1.204	1.000	1.83	2.805	2.391
0.79	1.201	0.987	1.85	2.816	2.414
0.81	1.199	0.975	1.87	2.825	2.437
0.83	1.200	0.965	1.89	2.832	2.458
0.85	1.203	0.955	1.91	2.838	2.478
0.87	1.208	0.947	1.93	2.842	2.496
0.89	1.215	0.939	1.95	2.845	2.513
0.91	1.225	0.934	1.97	2.847	2.528
0.93	1.238	0.931	1.99	2.848	2.542
0.95	1.253	0.928	2.01	2.850	2.554
0.97	1.271	0.925	2.03	2.848	2.564
0.99	1.292	0.924	2.05	2.846	2.573
1.01	1.316	0.924	2.07	2.842	2.581
1.03	1.342	0.927	2.09	2.838	2.585
1.05	1.372	0.932	2.11	2.834	2.587
1.07	1.404	0.940	2.13	2.828	2.588
1.09	1.438	0.953	2.15	2.822	2.586
1.11	1.475	0.971	2.17	2.816	2.581
1.13	1.514	0.999	2.19	2.809	2.574
1.15	1.555	1.037	2.21	2.801	2.565
1.17	1.599	1.080	2.23	2.793	-
1.19	1.644	1.127	2.25	2.784	-
1.21	1.691	1.179	2.27	2.775	-
1.23	1.739	1.235	2.29	2.766	-
1.25	1.788	1.292	2.31	2.756	-
1.27	1.837	1.352	2.33	2.746	-
1.29	1.888	1.410	2.35	2.736	-
1.31	1.936	1.466	2.37	2.725	-
1.33	1.984	1.522	2.39	2.714	-
1.35	2.031	1.577	2.41	2.703	-
1.37	2.077	1.629	2.43	2.692	-
1.39	2.122	1.678	2.45	2.680	-
1.41	2.165	1.726	2.47	2.669	-
1.43	2.208	1.771	2.49	2.657	-
1.45	2.250	1.814	2.51	2.645	-
1.47	2.292	1.856	2.53	2.633	-
1.49	2.333	1.895	2.55	2.620	-
1.51	2.374	1.933	2.57	2.608	-
1.53	2.413	1.969	2.59	2.596	-
1.55	2.452	2.004	2.61	2.583	-
1.57	2.490	2.037	2.63	2.571	-
1.59	2.528	2.069	2.65	2.558	-

Table A2. ($P-Y$, $Y-S$) relations for luminosity class III.

$Y-S$	$(P-Y)_n$	$(P-Y)_m$	$Y-S$	$(P-Y)_n$	$(P-Y)_m$
0.40	1.215	-	1.64	2.652	1.599
0.42	1.232	-	1.66	2.697	1.634
0.44	1.247	-	1.68	2.740	1.670
0.46	1.258	-	1.70	2.783	1.706
0.48	1.267	-	1.72	2.824	1.742
0.50	1.274	-	1.74	2.865	1.780
0.52	1.278	-	1.76	2.905	1.817
0.54	1.281	-	1.78	2.944	1.855
0.56	1.281	-	1.80	2.982	1.893
0.58	1.281	-	1.82	3.020	1.931
0.60	1.279	1.150	1.84	3.058	1.970
0.62	1.276	1.132	1.86	3.094	2.009
0.64	1.272	1.116	1.88	3.130	2.047
0.66	1.268	1.100	1.90	3.165	2.086
0.68	1.263	1.085	1.92	3.200	2.125
0.70	1.258	1.072	1.94	3.233	2.163
0.72	1.254	1.059	1.96	3.265	2.202
0.74	1.249	1.047	1.98	3.296	2.240
0.76	1.244	1.036	2.00	3.326	2.278
0.78	1.238	1.026	2.02	3.354	2.315
0.80	1.234	1.018	2.04	3.381	2.352
0.82	1.233	1.010	2.06	3.405	2.389
0.84	1.234	1.003	2.08	3.428	2.425
0.86	1.238	0.997	2.10	3.445	2.461
0.88	1.245	0.992	2.12	3.460	2.496
0.90	1.253	0.988	2.14	3.472	2.530
0.92	1.264	0.986	2.16	3.482	2.563
0.94	1.277	0.984	2.18	3.489	2.596
0.96	1.290	0.983	2.20	3.493	2.628
0.98	1.305	0.984	2.22	3.495	2.659
1.00	1.321	0.985	2.24	3.495	2.689
1.02	1.340	0.988	2.26	3.492	2.718
1.04	1.361	0.992	2.28	3.488	2.746
1.06	1.384	0.997	2.30	3.480	2.773
1.08	1.409	1.002	2.32	3.471	2.798
1.10	1.436	1.009	2.34	3.460	2.823
1.12	1.465	1.018	2.36	3.447	2.846
1.14	1.496	1.027	2.38	3.432	2.867
1.16	1.529	1.037	2.40	3.415	2.888
1.18	1.564	1.049	2.42	3.396	2.906
1.20	1.601	1.062	2.44	3.375	2.924
1.22	1.640	1.076	2.46	3.353	2.939
1.24	1.681	1.091	2.48	3.329	2.953
1.26	1.723	1.107	2.50	3.304	2.966
1.28	1.767	1.124	2.52	3.277	2.976
1.30	1.812	1.143	2.54	3.249	2.985
1.32	1.858	1.163	2.56	3.219	2.992
1.34	1.906	1.184	2.58	3.188	2.997
1.36	1.955	1.206	2.60	3.156	3.000
1.38	2.004	1.227	2.62	3.123	-
1.40	2.055	1.248	2.64	3.089	-
1.42	2.105	1.272	2.66	3.053	-
1.44	2.157	1.296	2.68	3.017	-
1.46	2.209	1.322	2.70	2.980	-
1.48	2.262	1.348	2.72	2.942	-
1.50	2.314	1.376	2.74	2.903	-
1.52	2.366	1.405	2.76	2.864	-
1.54	2.416	1.435	2.78	2.823	-
1.56	2.465	1.466	2.80	2.783	-
1.58	2.513	1.498	2.82	2.742	-
1.60	2.560	1.531	2.84	2.700	-
1.62	2.607	1.565	2.86	2.658	-

Table A3. ($P-X$, $Y-V$) and ($X-Y$, $Y-V$) relations for luminosity class V.

$Y-V$	$(P-X)_n$	$(P-X)_m$	$(X-Y)_n$	$(X-Y)_m$	$Y-V$	$(P-X)_n$	$(P-X)_m$	$(X-Y)_{rlap_n}$	$(X-Y)_m$
0.30	0.767	0.737	0.490	0.422	0.78	1.112	0.795	1.520	1.226
0.32	0.744	0.700	0.502	0.423	0.80	1.126	0.830	1.573	1.269
0.34	0.716	0.663	0.516	0.423	0.82	1.135	0.862	1.618	1.310
0.36	0.686	0.625	0.532	0.422	0.84	1.140	0.890	1.654	1.350
0.38	0.657	0.585	0.550	0.422	0.86	1.140	0.918	1.682	1.388
0.40	0.631	0.544	0.570	0.423	0.88	1.137	0.943	1.705	1.423
0.42	0.608	0.504	0.593	0.426	0.90	1.132	0.966	1.722	1.454
0.44	0.592	0.464	0.618	0.433	0.92	1.125	0.985	1.733	1.482
0.46	0.582	0.426	0.644	0.444	0.94	1.115	1.002	1.741	1.501
0.48	0.580	0.391	0.675	0.459	0.96	1.105	1.014	1.744	1.513
0.50	0.586	0.362	0.709	0.483	0.98	1.094	1.023	1.743	1.517
0.52	0.600	0.341	0.748	0.516	1.00	1.083	1.027	1.739	1.510
0.54	0.622	0.330	0.792	0.555	1.02	1.071	1.027	1.732	1.491
0.56	0.652	0.333	0.839	0.599	1.04	1.059	-	1.722	-
0.58	0.690	0.352	0.888	0.648	1.06	1.047	-	1.711	-
0.60	0.733	0.393	0.941	0.703	1.08	1.034	-	1.698	-
0.62	0.780	0.442	0.997	0.765	1.10	1.022	-	1.685	-
0.64	0.831	0.495	1.058	0.831	1.12	1.009	-	1.670	-
0.66	0.883	0.547	1.122	0.898	1.14	0.995	-	1.656	-
0.68	0.934	0.595	1.190	0.959	1.16	0.981	-	1.642	-
0.70	0.981	0.641	1.262	1.019	1.18	0.965	-	1.628	-
0.72	1.024	0.683	1.334	1.075	1.20	0.948	-	1.616	-
0.74	1.062	0.723	1.399	1.129	1.22	0.928	-	1.606	-
0.76	1.090	0.760	1.461	1.179	1.24	0.906	-	1.598	-

Table A4. ($P-X$, $Y-V$) and ($X-Y$, $Y-V$) relations for luminosity class III.

$Y-V$	$(P-X)_n$	$(P-X)_m$	$(X-Y)_n$	$(X-Y)_m$	$Y-V$	$(P-X)_n$	$(P-X)_m$	$(X-Y)_n$	$(X-Y)_m$
0.20	0.847	-	0.347	-	0.78	1.017	0.566	1.330	0.834
0.22	0.847	-	0.378	-	0.80	1.058	0.585	1.383	0.862
0.24	0.840	-	0.407	-	0.82	1.098	0.606	1.435	0.889
0.26	0.827	-	0.433	-	0.84	1.137	0.631	1.489	0.917
0.28	0.810	-	0.457	-	0.86	1.173	0.656	1.542	0.945
0.30	0.789	0.730	0.480	0.388	0.88	1.207	0.682	1.596	0.972
0.32	0.766	0.691	0.501	0.392	0.90	1.239	0.709	1.649	0.998
0.34	0.741	0.656	0.522	0.398	0.92	1.268	0.736	1.702	1.024
0.36	0.715	0.624	0.542	0.406	0.94	1.295	0.763	1.754	1.050
0.38	0.690	0.595	0.562	0.415	0.96	1.318	0.790	1.805	1.075
0.40	0.667	0.569	0.582	0.426	0.98	1.338	0.817	1.854	1.101
0.42	0.645	0.546	0.602	0.438	1.00	1.356	0.843	1.901	1.127
0.44	0.627	0.527	0.624	0.452	1.02	1.371	0.870	1.946	1.153
0.46	0.613	0.510	0.650	0.467	1.04	1.383	0.895	1.987	1.179
0.48	0.603	0.496	0.678	0.483	1.06	1.393	0.920	2.023	1.204
0.50	0.599	0.485	0.708	0.500	1.08	1.400	0.945	2.049	1.230
0.52	0.601	0.476	0.741	0.519	1.10	1.405	0.968	2.068	1.256
0.54	0.608	0.470	0.775	0.539	1.12	1.409	0.990	2.081	1.282
0.56	0.622	0.466	0.812	0.559	1.14	1.411	1.011	2.086	1.308
0.58	0.641	0.465	0.852	0.581	1.16	1.412	1.030	2.084	1.333
0.60	0.665	0.466	0.893	0.604	1.18	1.409	1.048	2.075	1.359
0.62	0.694	0.469	0.937	0.627	1.20	1.404	1.064	2.059	1.385
0.64	0.728	0.475	0.982	0.651	1.22	1.399	1.079	2.035	1.411
0.66	0.766	0.482	1.030	0.676	1.24	1.395	1.091	2.003	1.436
0.68	0.806	0.491	1.078	0.701	1.26	1.392	1.101	1.963	1.462
0.70	0.848	0.503	1.128	0.727	1.28	1.389	1.109	1.915	1.488
0.72	0.890	0.516	1.177	0.753	1.30	1.386	1.114	1.858	1.514
0.74	0.933	0.531	1.228	0.780	1.32	1.385	-	1.792	-
0.76	0.975	0.547	1.279	0.807	1.34	1.384	-	1.717	-